



# Mechanical and barrier properties of MOCVD processed alumina coatings on Ti6Al4V titanium alloy

Y. Balcaen<sup>a</sup>, N. Radutoiu<sup>a</sup>, J. Alexis<sup>a,\*</sup>, J.-D. Beguin<sup>a</sup>, L. Lacroix<sup>a</sup>, D. Samélor<sup>b</sup>, C. Vahlas<sup>b</sup>

<sup>a</sup> Université de Toulouse, LGP-ENIT/INPT, 47 avenue d'Azereix, BP 1629, 65016 Tarbes, France

<sup>b</sup> Université de Toulouse, CIRIMAT/INPT, 4 allée Emile Monso BP 44362, 31030 Toulouse cedex 4, France

## ARTICLE INFO

Available online 2 October 2011

### Keywords:

CVD  
Alumina  
Mechanical properties  
Adhesion  
Hot salt corrosion

## ABSTRACT

This study focuses on the implementation of different aluminum oxide coatings processed by metal-organic chemical vapor deposition from aluminum tri-isopropoxide on commercial Ti6Al4V titanium alloy to improve its high temperature corrosion resistance. Films grown at 350 °C and at 480 °C are amorphous and correspond to formulas  $\text{AlOOH}$ , and  $\text{Al}_2\text{O}_3$ , respectively. Those deposited at 700 °C are composed of  $\gamma\text{-Al}_2\text{O}_3$  nanocrystals dispersed in a matrix of amorphous alumina. Their mechanical properties and adhesion to the substrates were investigated by indentation, scratch and micro tensile tests. Hardness and rigidity of the films increase with increasing deposition temperature. The hardness of the coatings prepared at 350 °C and 480 °C is  $5.8 \pm 0.7$  GPa and  $10.8 \pm 0.8$  GPa respectively. Their Young's modulus is  $92 \pm 8$  GPa (350 °C) and  $155 \pm 6$  GPa (480 °C). Scratch tests cause adhesive failures of the films grown at 350 °C and 480 °C whereas cohesive failure is observed for the nanocrystalline one, grown at 700 °C. Micro tensile tests show a more progressive cracking of the latter films than on the amorphous ones. The films allow maintaining good mechanical properties after corrosion with NaCl deposit during 100 h at 450 °C. After corrosion test only the film deposited at 700 °C yields an elongation at break comparable to that of the as processed samples without corrosion. The as established processing–structure–properties relation paves the way to engineer MOCVD aluminum oxide complex coatings which meet the specifications of the high temperature corrosion protection of titanium alloys with regard to the targeted applications.

© 2011 Elsevier B.V. All rights reserved.

## 1. Introduction

Lightweight titanium alloys find nowadays potential use in numerous domains involving advanced materials for jet engine, other aerospace applications, desalination plants, orthopedic or dental implants and sporting goods. However, in addition to the elevated cost of such alloys, their implementation is hindered by their limited resistance to salt corrosion at high temperatures, when operation in such environments is part of the specifications of the material. It has been difficult until now to protect titanium alloys with coatings showing satisfactory behavior in terms of adhesion and substrate protection against stress corrosion cracking. These situations concern, for example the spinning centrifugal turboshaft engine, manufactured in Ti6Al4V titanium based commercial alloy. This part of the engine is very susceptible to oxidation and hard to protect. It is indeed generally not enough protected. For this reason, it suffers from a fairly high attrition rate and needs detailed periodic inspections. The presence of salt combined with strong mechanical stress generates hot salt stress corrosion phenomena (HSSC), which can lead titanium alloys to an untimely

failure. It is generally accepted that hydrogen is the major cause of embrittlement through a mechanism involving four steps: substrate corrosion, hydrogen generation, substrate embrittlement and crack initiation and propagation. Application of protective coatings on titanium alloys may improve their corrosion resistance and subsequently maintain their mechanical properties in corrosive, high temperature environment.  $\text{Al}_2\text{O}_3$  has received recent attention due to its surface and barrier properties, allowing for its use as catalytic support and as protective coating with enhanced mechanical properties and chemical durability. In addition to its numerous allotropic modifications and to the subsequent large spectrum of structure–properties relationships,  $\text{Al}_2\text{O}_3$  can be processed in the amorphous state and remain amorphous in a large temperature range. Metalorganic Chemical Vapor Deposition (MOCVD) of alumina has been reported many times in the literature. However, only a few works explicitly deal with the deposition of amorphous alumina films [1]. Significant work has been provided by the authors in the recent years in this field. Especially, the relation between the operating conditions of Metalorganic Chemical Vapor Deposition (MOCVD) and the characteristics of the obtained amorphous  $\text{Al}_2\text{O}_3$  coatings, including the modeling of the process considering appropriate chemical kinetic schemes [1–6] was discussed. The rationale of these investigations is based on two pillars: the first concerns the moderate deposition temperature which is compatible with the thermal loads the substrate can

\* Corresponding author. Tel.: +33 562442723; fax: +33 562442708.  
E-mail address: [joel.alexis@enit.fr](mailto:joel.alexis@enit.fr) (J. Alexis).

tolerate without modification of its microstructure and, consequently of its properties and performance. The second is based on the excellent barrier properties of the amorphous alumina films allowing for efficient protection of easily oxidized light weight alloys such as the titanium (and possibly magnesium) based ones. Indeed, preliminary investigation of combined thermal, mechanical and chemical stresses applied on physical vapor deposited (PVD) SiC and Si<sub>3</sub>N<sub>4</sub>, and of MOCVD amorphous Al<sub>2</sub>O<sub>3</sub> coatings on Ti6242 alloys, revealed that the first two suffered from severe damage resulting in less efficient protection of the alloy, while only the latter maintained its integrity (except minor damage in the form of localized small pits and subsequent local spallation of the films) [7,8]. It was concluded that understanding and improving the mechanical compatibility was the key factor for the Al<sub>2</sub>O<sub>3</sub>/Ti system to corrosion protection.

Based on the above, the objective of this study is to make further progress in the establishment of the correlation between the characteristics of the coatings and their capacity to protect the Ti6Al4V alloy in conditions that are at least as severe as the ones prevailing during its targeted operation. The work consists of depositing on Ti6Al4V aluminum oxide films of three different microstructures, namely amorphous aluminum oxyhydroxide ALOOH, amorphous aluminum oxide Al<sub>2</sub>O<sub>3</sub> and Al<sub>2</sub>O<sub>3</sub> oxide composed of amorphous and nanocrystalline domains. The three coatings are processed under different conditions and are expected to provide coating/substrate couples with different combined thermal, mechanical and chemical behaviors with regard to preestablished specifications. In this way, it is expected to reveal the mechanical behavior of the metal/oxide interface per se, thus defining in a subsequent step appropriate combinations of surface functionalization — film characteristics leading to an integrated surface engineering of the Ti6Al4V alloy.

In the following, the processing parameters and mechanical tests carried out will be introduced first. Then, the intrinsic mechanical properties and the adhesion of coatings will be presented and discussed with regard to their deposition temperature, before providing concluding remarks.

## 2. Material and methods

### 2.1. Material

MOCVD of alumina coatings was performed in a tubular, horizontal hot-wall reactor at 666 Pa and at temperatures between 350 °C and 700 °C. Aluminum triisopropoxide (ATI) was thermoregulated in a bubbler at 100 °C and was carried to the deposition zone, with 99.9992% pure nitrogen as carrier gas. Table 1 resumes the processing conditions. It is recalled that under such conditions, the composition, microstructure and crystallinity of the alumina films strongly depend on the deposition temperature. These grown in the range 350 °C–415 °C are amorphous and partially hydroxylated AlO<sub>1+x</sub>(OH)<sub>1–2x</sub> with x varying from 0 (ALOHH) at 350 °C to 0.5 (Al<sub>2</sub>O<sub>3</sub>) at 415 °C. Those processed between 415 °C and 650 °C are composed of amorphous Al<sub>2</sub>O<sub>3</sub> and those processed around 700 °C contains γ-Al<sub>2</sub>O<sub>3</sub> nanocrystals distributed in an amorphous Al<sub>2</sub>O<sub>3</sub> matrix. The film thickness is approximately 1 μm.

**Table 1**  
Processing conditions for the growth of Al<sub>2</sub>O<sub>3</sub> coatings.

Growth temperature (°C)	350–700
Pressure (Pa)	666
Carrier gas flow rate (N <sub>2</sub> , sccm)	20
Dilution gas flow rate (N <sub>2</sub> , sccm)	632
Total gas flow rate (sccm)	652
ATI bubbler temperature (°C)	100
ATI molar fraction (10 <sup>–3</sup> )	2.35
Deposition time (min)	5–60
Substrate (10 × 15 mm)	Ti6Al4V

### 2.2. Methods

A detailed description of the compositional and structural analysis of the as deposited films is presented in [5]. A nanoindenter XP from MTS was used with a Dynamic Contact Module (DCM) to determine the hardness. On each coating, a matrix of 20 measurements in the Continuous Stiffness mode was carried out with a Berkovich indenter by fixing a maximum in-depth displacement of 300 nm. In order to overcome the influence of the substrate, taking into account the roughness, the interval for calculating the properties of the deposits varies between 30 and 100 nm. The Young's modulus of the coatings was calculated starting from the contact stiffness (Eq. (1)) [9].

$$S_e = \frac{2}{\sqrt{\pi}} E_r \sqrt{A(h_c)} \quad (1)$$

$S_e$  is the stiffness of contact determined in the higher part of the unloading curve,  $A(h_c)$  the contact area as a function of the indentation depth.  $E_r$  is the reduced modulus of the system holding account of the Young's moduli and the Poisson's ratios of indenter ( $E_i$ ,  $\nu_i$ ) and of the sample ( $E_e$ ,  $\nu_e$ ) (Eq. (2)). To calculate  $E_e$ , the Poisson's ratio  $\nu_e$  was set to 0.2.

$$\frac{1}{E_r} = \frac{1-\nu_i^2}{E_i} + \frac{1-\nu_e^2}{E_e} \quad (2)$$

The quantitative determination of the adhesive strength is difficult or even impossible due to the adherence and thickness of the coatings [10]. Moreover, there is a multitude of adherence tests, more or less simple, more or less qualitative. More than 355 different tests have been compiled by Mittal [11]. The choice of a test depends on its application. It must be as simple as possible to implement and pertinent; its parameters must be known and controlled. Taking into account these criteria, micro tensile tests and micro scratch tests were used for the determination of the adhesion of the coatings. Micro tensile tests were performed with a KUSTOM TS 250 designed to be used in a JEOL JSM6400 scanning electron microscope. The setup allows 250 daN and 4 mm maximum load and elongation of the sample, respectively. 0.6 mm-thick samples with useful area of 7 × 2 mm<sup>2</sup> were elongated at a 0.6 mm/min rate. According to Ohmura and Matsuoka [12], the more important the crack density is at the end of the test, the higher is the adherence. Based on this fragile behavior, the adhesion of the coatings can be estimated using the model suggested by Agrawal and Raj [13] which allows calculating the value of the critical shear stress,  $\tau$ , before the delamination of the coating (Eq. (3)).

$$\tau = \frac{\pi e_f}{\lambda} \sigma \quad (3)$$

$e_f$  is the film thickness and  $\lambda$  is the wavelength of the sinus function defining the shear force at the substrate–deposit interface.  $\lambda = 2\lambda_0$  corresponds to the distance between two cracks when the sample surface is cracks saturated,  $\sigma$  is the maximum normal stress supported by the film. According to Chen et al. [14,15] the maximum normal effective stress in the film, considering the internal stresses, is:

$$\sigma = \sigma_a + \sigma_r \quad (4)$$

$\sigma_a$  is the stress when the first crack appears and  $\sigma_r$  the residual stress of the film. Considering that the film is fragile, it is assumed that  $\sigma_a + E_f \varepsilon_f$ . Thus  $\tau$  equals:

$$\tau = \frac{\pi e_f}{2\lambda_0} \cdot (E_f \varepsilon_f + \sigma_r) \quad (5)$$

Scratch adhesion testing was carried out using a CSEM® commercial microscratch instrument. A Rockwell C diamond indenter with a

200  $\mu\text{m}$  radius was used at a scratch speed of 10 mm/min. During each scratch test, the normal load was continuously increased from 30 mN at a loading rate of 100 N/min until severe interfacial failure occurred. The critical normal load,  $L_c$ , corresponding to the initiation of the interfacial failure, was detected by a sudden increase in acoustic emission and was confirmed by observation with a scanning electron microscope (SEM-FEG JEOL 7000F). SEM observations and Energy Dispersive X-ray analysis (SDD BRUKER — 129 eV) allowed to determine the type of debonding (adhesive or cohesive). Hot salt corrosion tests were performed on uncoated and coated samples after deposition of NaCl. This deposition was performed by applying a calibrated droplet of saline solution on the surface of the sample. The NaCl solution was prepared with natural sea salt and deionized water. Salt crystallization on the tested surface was obtained by maintaining the sample in an oven for 5 min at 115 °C. This procedure allows obtaining reproducible application of the salt. The deposited mass of NaCl was 120  $\mu\text{g}$  with a local salt concentration of 3 mg/cm<sup>2</sup>. This value is 10 times greater than the salt concentration present in engines exposed to severe service conditions [16]. After the salt deposition, the sample was introduced in a furnace at 450 °C during 100 h. This temperature was determined based on the maximum operating temperature of the targeted application. After the experiment, the degradation of the mechanical properties (maximum strength, yield strength, ductility) of the tensile samples was evaluated. The results were combined with postmortem fractographic studies, and were compared with the intrinsic properties of the coatings and with their adhesion to the substrate.

### 3. Results and discussion

The microstructure of the coatings is illustrated by the cross-sectional scanning electron micrographs of Fig. 1. The coatings deposited at 350 °C and 480 °C are compact and free of porosity and grain boundaries. This microstructure is significantly different from that of the coating prepared at 700 °C, which is composed of columnar grains, oriented perpendicularly to the substrate surface. Fig. 2 presents the loading and unloading curves of nanoindentation tests. In order to reach the predetermined depth of 300 nm, the applied load varied with the nature of the coating: it was equal to 3.5 mN, 11 mN and 1 mN for the coatings deposited at 350 °C, 480 °C and 700 °C, respectively. There is a clear distinction between the low temperature processed samples and the one processed at 700 °C. The former present better mechanical properties when the latter seems to present lower rigidity and hardness. Tests performed on the coatings deposited at 350 °C and at 480 °C are reproducible in contrast with those performed on coatings deposited at 700 °C. Moreover, the loading–unloading curves of the coatings processed at 700 °C are not so reproducible and present numerous inflection points induced by the limited cohesion of the coating and its roughness. Thus, no quantitative values of mechanical properties are given for the coating processed at 700 °C.

The ratio of the elementary work values of the elastic and the total deformation during indentation was estimated for the coatings elaborated at 350 °C and 480 °C. Both energies were calculated from the areas under the load vs. displacement curves (Eq. (6)).

$$W_{(J)} = d_{(m)} \times F_{(N)} \quad (6)$$

Table 2 resumes the calculated areas for the two coatings. Calculated values of hardness and Young's modulus are also reported in this table. It appears that the ratio of the elastic energy over the total energy decreases with increasing the deposition temperature. The values of hardness and rigidity determined by the dynamic nanoindentation tests are well below those given for the bulk alumina. This difference may be attributed either to the nanoindentation technique used, or to the influence of the substrate, or to the structure

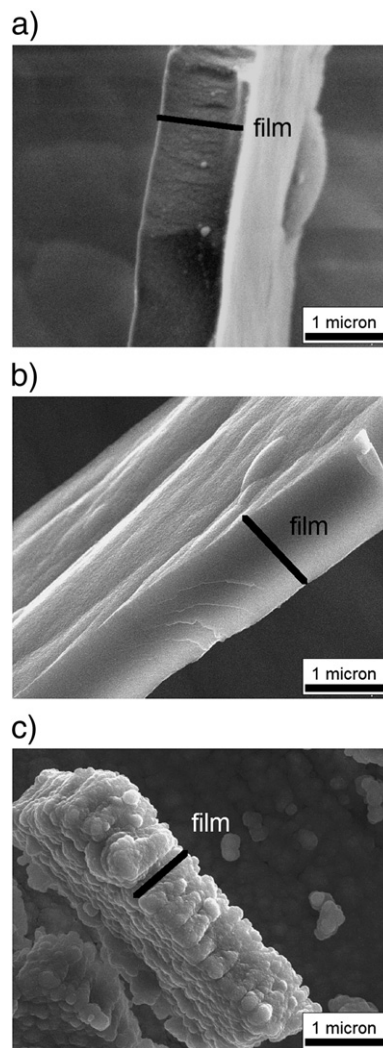


Fig. 1. Cross-sectional scanning electron micrographs of the coatings processed at 350 °C (a), 480 °C (b) and 700 °C (c).

of the coatings. For this reason, nanoindentation tests were also performed on commercial bulk alumina and on the same coatings deposited on silicon (Fig. 3). The hardness and Young's modulus obtained by nanoindentation on bulk samples are consistent with the results given in literature [17]. The hardness and the rigidity of 92% and 96% pure alpha alumina are equal to  $H_{92\%} = 20 \pm 6$  GPa,  $E_{92\%} = 320 \pm 50$  GPa and  $H_{96\%} = 33 \pm 3$  GPa,  $E_{96\%} = 423 \pm 37$  GPa, respectively. Whatever the nature of the substrate, the hardness and rigidity of the films increased with increasing the deposition temperature up to 480 °C. In addition, the hardness and Young's modulus of coatings prepared on silicon substrate confirm the values obtained for the coatings on titanium substrate. Therefore, the nanoindentation technique and the selected test parameters are relevant and the low values obtained for the coatings compared to bulk alpha alumina are attributed to differences of the microstructure of the samples. Depending on the deposition temperature, the increased hardness and rigidity seem to correspond mainly to an increase in the purity of the amorphous alumina deposits. Haanappel et al. also showed that the hardness of alumina coatings prepared by Low Pressure MOCVD and Atmospheric pressure MOCVD increases when the deposition temperature increases from 250 °C to 450 °C [18]. They attribute this increase to the disappearance of the amount of the OH group and in particular to the decrease of boehmite ( $\text{AlO}(\text{OH})$ ).

Insight in the intrinsic properties of the coatings allows determining their adhesion to the substrate.



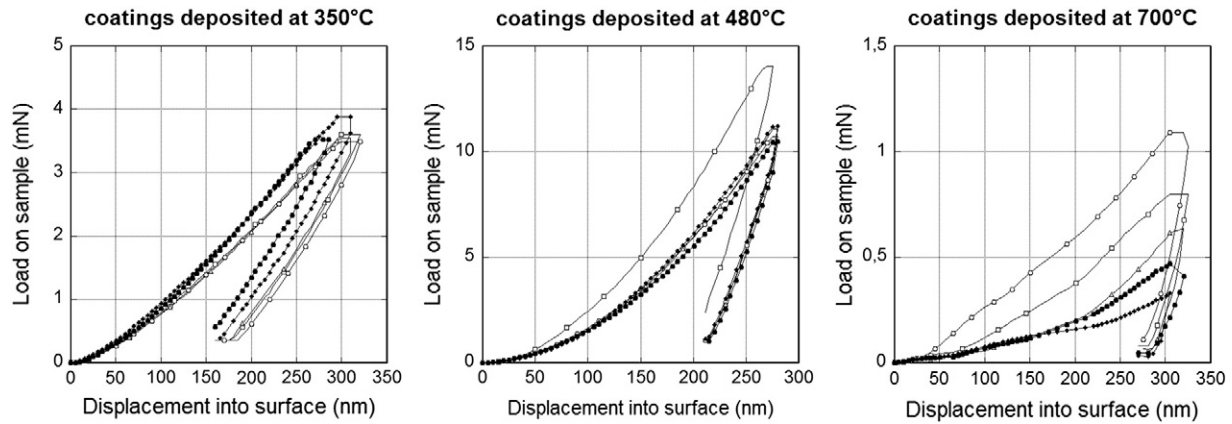


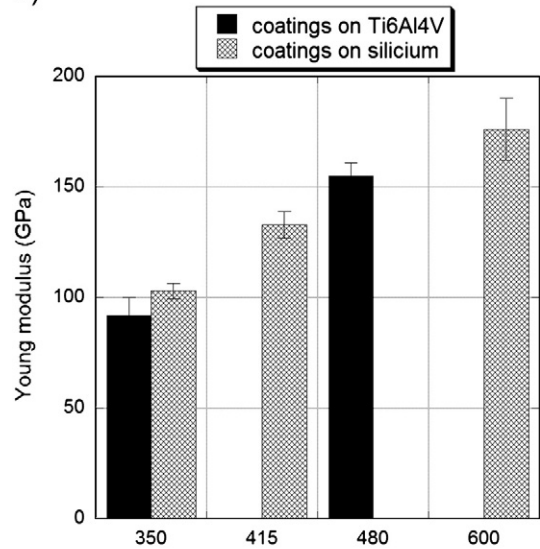
Fig. 2. Loading and unloading curves of nanoindentation tests performed on coatings for different deposition temperatures.

Fig. 4 presents the measured critical load of failure ( $L_{ci}$ ) of the coatings elaborated at 350 °C and at 480 °C and SEM micrographs of scratches on coatings elaborated at 350 °C (Fig. 4a), 480 °C (Fig. 4b) and 700 °C (Fig. 4c). Such observations allow determining the type of failure of these coatings. Coatings prepared at 350 °C and at 480 °C present a typical mechanical behavior of a hard and brittle ceramic coating film deposited on soft metallic substrate. For each type of damage observed, a critical load of adhesion ( $L_{ci}$ ) is defined. Lateral cracking ( $L_{c1}$ ) appears at low load, followed by side ( $L_{c2}$ ) and frontal cracks ( $L_{c3}$ ). Then fragmentation of the coating ( $L_{c4}$ ) and finally important spallation ( $L_{c5}$ ) occur. Regardless of the type of damage  $L_{ci}$  is higher for coatings processed at 480 °C, resulting in a better adhesion of these coatings than that of coatings processed at 350 °C (Fig. 4). This is particularly obvious for heavy load, when spallation appears. The film deposited at 700 °C presents a different mechanical behavior from the other two: it gets damaged already after the pre-scan pass (a load of 0.03 N). Optical microscopy and SEM reveal the wrenched material with small debris.

The above results reveal two scratch behaviors. The films prepared at 350 °C and at 480 °C present adhesive rupture at the interface without plastic deformation (Fig. 4a and b). The fracture behavior of the coating is clearly weak, with clear fracture patterns by cleavage (Fig. 1). The following scenario of failure is proposed to explain this finding. During the pass of the indenter, the coating located forward undergoes compression when the one located backward undergoes tension. The break presents as a crack crossing the coating to the substrate, perpendicular to the surface. When compression exceeds a critical value, the coating forms a “blister” forward and on the sides of the scratch. The stress becoming too high, the coating is broken in its entire thickness. Spallations escape or remain trapped under the indenter. Then, the main failure mode in the scratch testing of hard coatings processed at 350 °C or 480 °C is mainly buckling and wedge spallation.

The coating obtained at 700 °C (Fig. 4c) presents a very different scratch behavior from the other two. Unlike the other two, it cracks during the nanoindentation test, making it almost impossible to measure its mechanical properties. During the scratch tests it gets damaged with the pre scan passes (0.03 N load). This illustrates perfectly the

a)



b)

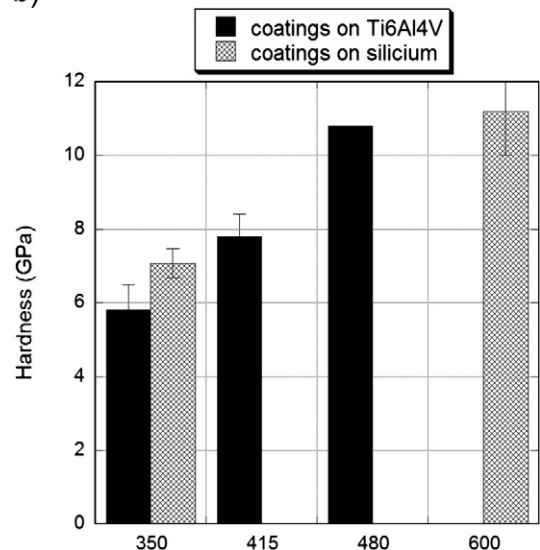
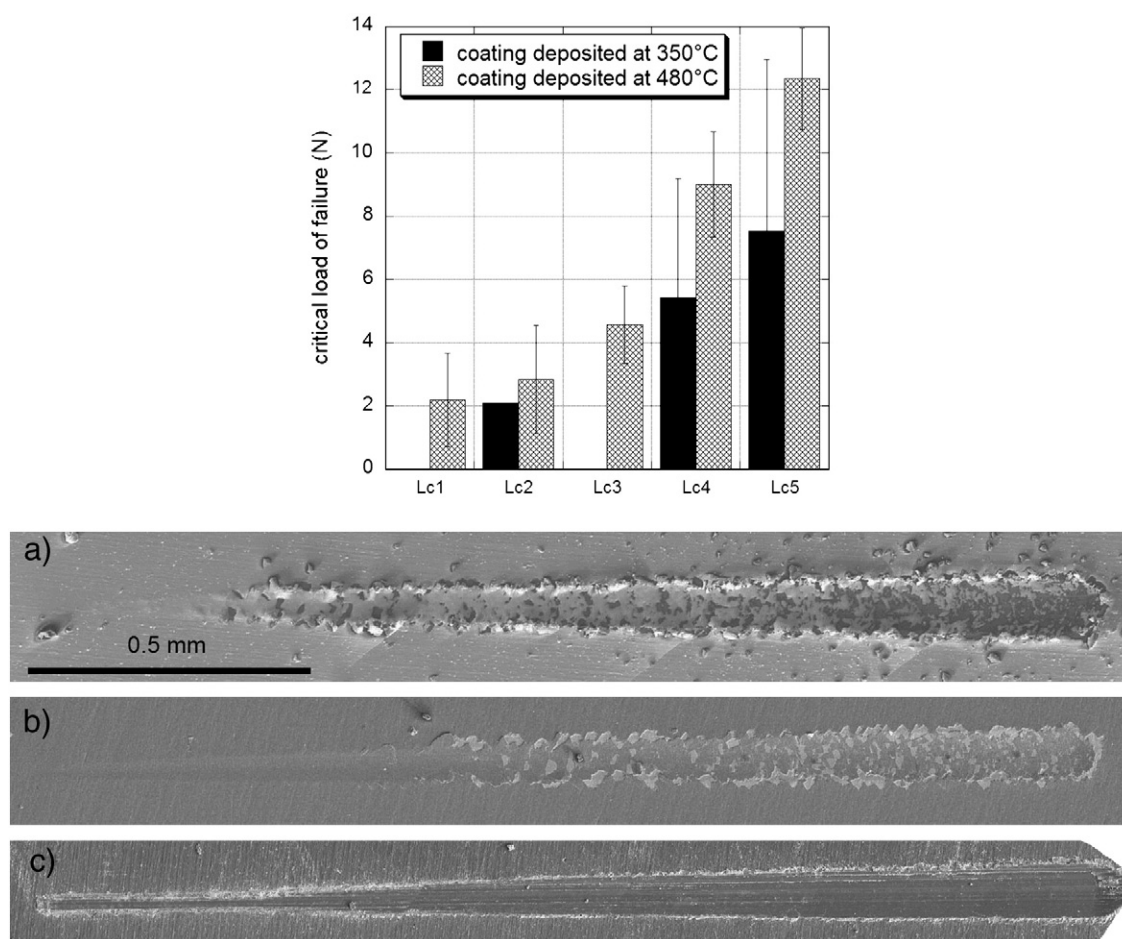


Fig. 3. Young's modulus (a) and hardness (b) of the coatings processed on Si and on Ti6Al4V for different deposition temperatures.

Table 2

Mechanical properties of the coatings as a function of the deposition temperature.

Deposition temperature (°C)	350	480
Total energy (pJ)	451	991
Elastic energy (pJ)	265	337
Plastic energy (pJ)	185	654
Ratio elastic energy/total energy	0.59	0.34
Young's modulus (GPa)	92 ± 8	155 ± 6
Hardness (GPa)	5.8 ± 0.7	10.8 ± 0.8



**Fig. 4.** Values of critical loads of failure  $L_{CI}$  of coatings processed at 350 °C and at 480 °C.  $L_{CI}$  for coatings processed at 700 °C is near zero. SEM observations of the scratches made on coatings elaborated at (a) 350 °C, (b) 480 °C and (c) 700 °C.

low cohesion of the film. In addition, its nodular structure contrasts sharply with that of others. However, a thin coating remains adherent to the substrate, even after the most severe scratching. During the scratch test, the deformation is mainly plastic deformation for the soft coating processed at 700 °C. No buckling failure mode is observed. In this case, the scratch test is not well suited to measure the adhesion and simply reveals that the interfacial shear strength is lower than the shear strength of the coating elaborated at 700 °C. The difference in scratch behavior depending on the temperature development can be explained by the intrinsic properties of the coatings and substrates. Coatings were classified according to the classification of Bull [19] (Fig. 5), i.e. the substrate hardness vs coatings hardness map.

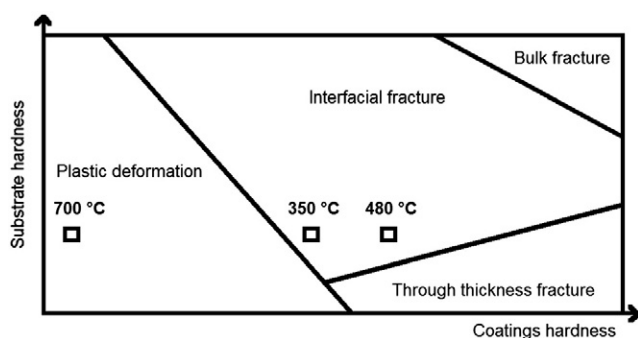


**Fig. 5.** Substrate hardness versus coatings hardness map, delimiting areas within which prevails particular failure mode of the coating revealed by the Bull scratch adhesion test.

The adhesion of the coatings was also estimated by micro tensile tests. The shear stress at the interface was calculated and presented in Table 3 by applying the formula of Agrawal and Raj (Eq. (3)). The distance between cracks was determined far away from the fracture zone by SEM after testing. Table 3 presents the results of shear stress evolution as a function of deposition temperature. The shear stress decreases with temperature development. This test confirms the previous results. The coating prepared at 350 °C seems more adherent than the coating prepared at 480 °C. The low shear stress determined for the coating prepared at 700 °C does not represent a value of adhesion but its cohesive strength as shown by SEM micrographs of the cracking pattern (Fig. 6). Energy Dispersive spectrometry X-ray analysis confirmed the presence of oxygen and aluminum on the coated tensile specimen at 700 °C after rupture and not on the others. The failure of coatings prepared at 350 °C and 480 °C is adhesive whereas the rupture of the coating prepared at 700 °C is cohesive. To corroborate this, the percentage of coating flaking on the substrate was determined by image analysis with the software AREAS Microvision from observations by scanning electron microscopy. The surface flaking

**Table 3**

Evolution of the shear stress at the interface as a function of the deposition temperature.

Deposition temperature (°C)	$\varepsilon_f$ (%)	$\sigma_R$ (MPa)	$\sigma_c$ (MPa)	$\delta$ ( $\mu$ m)	$\lambda$ ( $\mu$ m)	$\tau$ (MPa)
350	2.36	−69.5	1075	700	3.70	1249
480	2.16	−182.3	2026	880	14.34	610

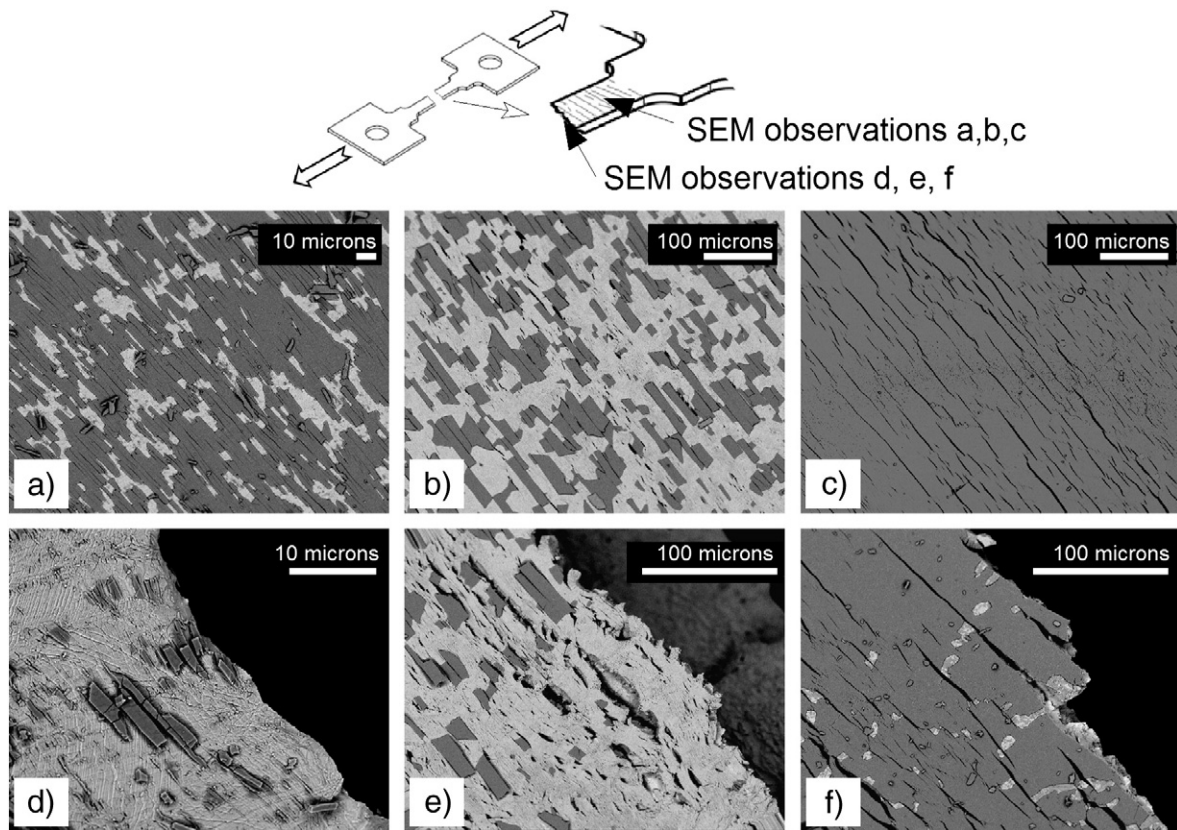


**Fig. 6.** Electron backscattered images of the surface of the samples after tensile tests: observations away from the rupture zone of the coatings deposited at (a) 350 °C, (b) 480 °C, (c) 700 °C; observations of the rupture zone of the coatings deposited at (d) 350 °C, (e) 480 °C, (f) 700 °C.

represents 17%, 55% and 0% respectively for deposits prepared at 350 °C, 480 °C and 700 °C.

Table 4 shows the influence of salt corrosion at high temperature on the mechanical properties of coated and uncoated Ti6Al4V alloy. As seen before, the saline corrosion test consists in the exposure of the specimen to salt attack during 100 h at 450 °C. First the influence of oxidation at 450 °C during 100 h was studied. No influence on the ultimate strength or on the ductility was observed. However, the bare Ti6Al4V alloy reveals, after saline corrosion test, a decrease of both the ultimate strength and the ductility revealing the well-known susceptibility of the Ti6Al4V alloy regarding to the salt attack. On the contrary, the yield strength of the coated specimens after is similar to that of the bare specimens before the saline corrosion test. The coatings can thus preserve the good mechanical properties of the Ti6Al4V alloy even after salt attack. However, only the coating prepared at 700 °C yields an elongation at break, after corrosion test, comparable to that of the specimen before the corrosion test. The Ti6Al4V alloy protected by the two other coatings exhibits a fall of ductility. This ductility is indeed 4.9% and 3.2% for the coating obtained at 350 and 480 °C respectively, instead of 11.1% for the bare Ti6Al4V alloy before the corrosion test.

Vickers hardness tests were carried out on cross-sectional areas of the shoulder for gripping of the tensile specimens to verify if the mechanical properties of the Ti6Al4V recorded during tensile tests are induced by hot corrosion tests or by microstructure changes induced by deposition heating at 350 °C, 480 °C or 700 °C. The hardness of the Ti6Al4V substrates is identical regardless of the coating made. The heating of samples during the deposition of coatings does not alter the mechanical properties of the Ti6Al4V alloy. Therefore, changes in mechanical properties were attributable to corrosion at high temperatures. Moreover, a Ti6Al4V specimen was tested for 100 h at 450 °C without salt corrosion; no decrease in mechanical properties is observed for this specimen. Therefore, the decrease in mechanical properties is induced by corrosion and non-oxidation at 450 °C. The specimens were then observed by scanning electron microscopy in order to understand the mechanisms of damage. The micrographs of Fig. 7 show the fracture surface.

The behavior of the coating prepared at 700 °C differs from the other two. It is indeed present even at the edge of the fracture surface. Only the surface which was exposed to NaCl was affected by hot salt corrosion. The other side (not corroded) and the heart seem ductile specimens. The proportion of ductile and brittle areas was estimated

**Table 4**

Influence of salt corrosion at high temperature on the mechanical properties of coated and uncoated samples.

Ti6Al4V	Test conditions	Yield strength (MPa)	Ductility (%)	Brittle area/ductile area
Not coated		850	11.13	0
Not coated	Oxidation – 450 °C/100 h – air	850	11.03	0.05
Not coated	Hot corrosion with NaCl – 450 °C/100 h – air	805	4.06	0.23
Coatings elaborated at 350 °C	Hot corrosion with NaCl – 450 °C/100 h – air	880	4.9	0.11
Coatings elaborated at 480 °C	Hot corrosion with NaCl – 450 °C/100 h – air	845	3.21	0.05
Coatings elaborated at 700 °C	Hot corrosion with NaCl – 450 °C/100 h – air	850	9.19	0.04



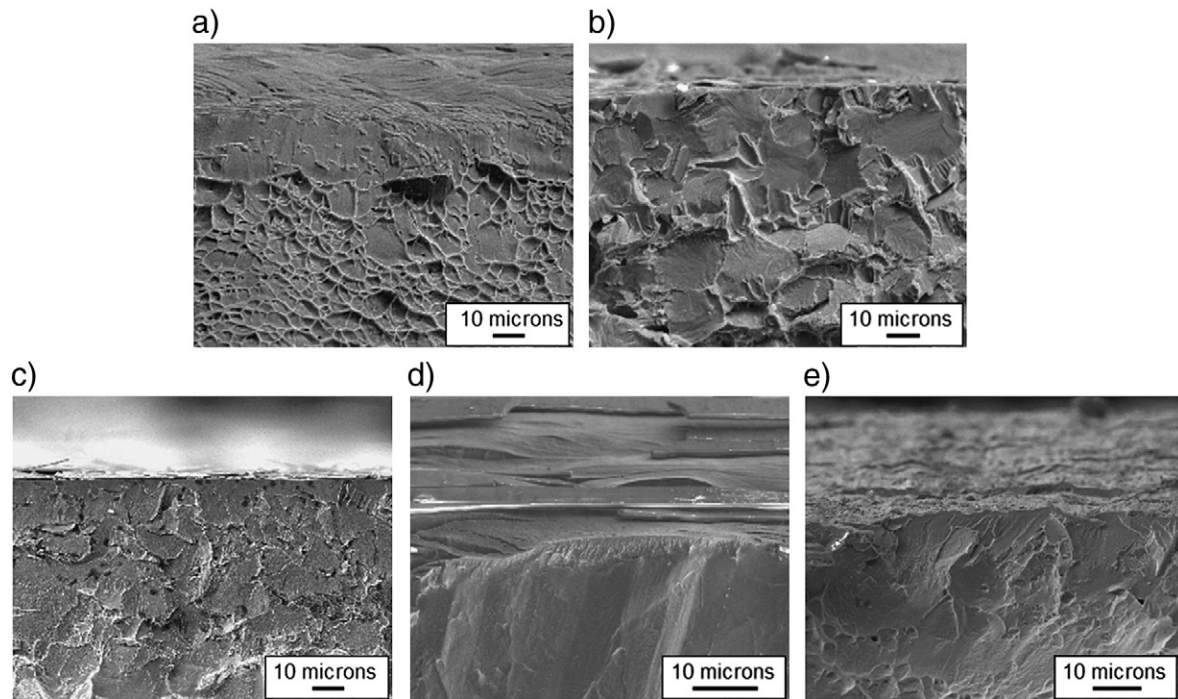


**Fig. 7.** Observations of fracture surfaces (a) Ti6Al4V – 100 h – 450 °C, (b) Ti6Al4V – corroded with NaCl – 100 h – 450 °C, (c) coatings deposited at 350 °C on Ti6Al4V – corroded with NaCl – 100 h – 450 °C, (d) coatings deposited at 480 °C on Ti6Al4V – corroded with NaCl – 100 h – 450 °C, (e) coatings deposited at 700 °C on Ti6Al4V – corroded with NaCl – 100 h – 450 °C.

by image analysis with the software AREAS Microvision (Table 4). The specimens with a coating prepared at 480 °C or 700 °C present a poor percentage of brittle area unlike the deposit prepared at 350 °C. With a deposit prepared at 480 °C and 700 °C, the percentage of area ratio percentage of fragile ductile zone is comparable to that of a non-corroded specimen heat treated 100 h at 450 °C.

#### 4. Conclusions

Completely amorphous and nanocrystalline/amorphous, stoichiometric and hydroxylated aluminum oxide coatings were processed on Ti6Al4V titanium alloy and on Si substrates by MOCVD. Their mechanical properties and adhesion to the substrates were investigated by indentation, scratch and micro tensile tests. Amorphous  $\text{Al}_2\text{O}_3$  coatings deposited at 480 °C present the highest hardness, equal to  $10.8 \pm 0.8$  GPa. Similar trends are obtained for the stiffness of the coatings. Adhesive and cohesive failure is observed for amorphous and nanocrystalline coatings, respectively. Progressive cracking is observed for the latter during micro tensile tests. The mechanical strength of the coated samples is similar to that of the as processed uncoated ones. After high temperature salt corrosion test, the mechanical strength of the coated Ti alloys is higher than that of the uncoated alloys, revealing that the films allow maintaining good mechanical properties in the targeted operating conditions. However, only the nanocrystalline coating supports the decrease of ductility recorded after corrosion test on Ti6Al4V. The as established processing–structure–properties relation paves the way to engineer MOCVD aluminum oxide complex coatings which meet the specifications of the high temperature corrosion protection of titanium alloys with regard to the targeted applications. The next step to meet this objective is the surface preparation of the substrate so as to accommodate the mechanical characteristics of the amorphous coatings;

i.e. the ones that present the best barrier properties. Beyond the protection of Ti6Al4V the present work is expected to be useful for the implementation of such surface treatments on other pieces, for example those used in wafer tool machining.

#### References

- [1] V.A.C. Haanappel, H.D. VanCorbach, R. Hofman, R.W.J. Morssinkhof, T. Fransen, P.J. Gellings, *High Temp. Mater. Processes* 15 (4) (1996) 245.
- [2] M.M. Sovar, D. Samelor, A.N. Gleizes, C. Vahlas, *Surf. Coat. Technol.* 201 (22–23) (2007) 9159.
- [3] M.M. Sovar, D. Samelor, A. Gleizes, P. Alphonse, S. Perisanu, C. Vahlas, *Adv. Mater. Res.* 23 (2007) 245.
- [4] A.M. Huntz, M. Andrieux, C. Vahlas, M.M. Sovar, D. Samelor, A.N. Gleizes, *J. Electrochem. Soc.* 154 (5) (2007) P63.
- [5] A.N. Gleizes, C. Vahlas, M.M. Sovar, D. Samelor, M.C. Lafont, *Chem. Vap. Depos.* 13 (2007) 23.
- [6] A. Gleizes, M.M. Sovar, D. Samelor, C. Vahlas, *Adv. Sci. Technol.* 45 (2006) 1184.
- [7] J.-D. Beguin, D. Samelor, A.N. Gleizes, J.A. Petit, B. Sheldon, *Mater. Sci. Forum* 595–598 (2008) 719.
- [8] J.D. Beguin, D. Adrian, J.A. Petit, J.P. Rivière, C. Vahlas, *Proceedings of the 20th International Conference on Surface Modification Technologies (ASM International)*, 2007, p. 59.
- [9] W.C. Oliver, G.M. Pharr, *J. Mater. Res.* 7–6 (1992) 1564.
- [10] H. Weiss, *Surf. Coat. Technol.* 71 (1995) 201.
- [11] K.L. Mittal, in: K.L. Mittal (Ed.), *Adhesion Measurement of Films and Coatings*, 1995, p. 1.
- [12] T. Ohmura, S. Matsuoka, *Surf. Coat. Technol.* 169–170 (2003) 728.
- [13] D.C. Agrawal, R. Raj, *Acta Metall.* 37 (1989) 1265.
- [14] B.F. Chen, J. Hwang, I.F. Chen, G.P. Yu, J.H. Huang, *Surf. Coat. Technol.* 126 (2000) 91.
- [15] B.F. Chen, J. Hwang, G.P. Yu, J.H. Huang, *Thin Solid Films* 352 (1999) 173.
- [16] R.L. Ashbrook, *Nasa Technical Note*, NASA TN D-4999 (1969).
- [17] M. Baucio, *ASM Engineered Materials Reference Book*, Second Edition, ASM International, Materials Park, OH, 1994.
- [18] V.A.C. Haanappel, D.v.d. Vendel, H.S.C. Metselaar, H.D. van Corbach, T. Fransen, P.J. Gellings, *Thin Solid Films* 254 (1995) 153.
- [19] S.J. Bull, *Tribol. Int.* 30 (7) (1997) 491.